Multi-Harmonic Analysis in a Floating Harmonic Probe Method for Diagnostics of Electron Energy and Ion Density in Low-Temperature Plasmas

Seiya Kito, Keiichiro Urabe [a], and Koji Eriguchi

Department of Aeronautics and Astronautics, Kyoto University, Kyoto-Daigaku Katsura, Nishikyo-ku, Kyoto 615-8540, Japan

[a] E-mail: urabe.keiichiro.3x@kyoto-u.ac.jp

Abstract: A floating harmonic probe (FHP) is used to measure the electron energy and ion density in plasmas. It applies an AC voltage to an electrically floated probe and measures harmonic frequency components in the probe current which contain information about the parameters. In this study, we have quantitatively investigated the effects of stray impedances in an FHP measurement system on the calculated parameters. We also discuss the influence of the electron energy distribution function (EEDF) when it deviates from a Maxwellian shape on the FHP measurement. A new approach of multi-harmonic analysis of FHP data (MHA-FHP) is proposed to analyze the electron energy in plasmas with non-Maxwellian EEDFs. The MHA-FHP method has been compared with the conventional FHP and Langmuir probe methods thorough the measurement of low-temperature argon plasmas. Experimental results indicated that the MHA-FHP method can provide the shape of the EEDFs, effective electron temperature, and ion density.

1. Introduction

Diagnostics of electron-related plasma parameters, such as electron density n_e and temperature T_e are essential for the research and development of low-temperature plasma technologies. These parameters govern electron-related inelastic collisions that generate ions, radicals, and excited species. Electrical probing methods are widely used to diagnose low-temperature plasmas generated in low-pressure gas atmospheres. The Langmuir probe (LP) method, which analyzes the current-voltage (I–V) characteristics of a metal probe inserted into the plasma, is one of the most common methods.[1,2)]

In low-temperature reactive plasmas used in material processes such as plasma-enhanced chemical vapor deposition (PECVD), it is difficult to adequately measure the parameters using DC-based electrostatic probing methods, including the LP method. This is because DC-based methods generally require the maintenance of a clean metallic-probe surface, i.e., a low-resistance contact between the probe and the ion sheath during the measurement.[3,4)] One approach to reactive plasma diagnostics is to avoid deposition or surface modification on the probe during the measurement by using a thin noble metal probe heated by an electric current flow.[5,6)] Another approach is to use AC-based methods that can obtain information on plasmas through dielectric materials on the probe. For example, the plasma absorption probe method is an AC-based technique developed for measuring n_e. It detects the resonant frequency between the surface wave on the dielectric cover of a probe antenna and the plasma oscillation.[7-9)]

The floating harmonic probe (FHP) method is also an AC-based measurement method that examines both electron energy and plasma density. In the FHP method, a kHz-order AC voltage is applied to an electrically floating probe. Due to the nonlinearity of the ion-sheath impedance, current components with harmonic frequencies of the applied AC voltage are generated and flow in the probe. In typical FHP measurements, the first and second-harmonic current amplitudes, T_e and the ion density n_i are derived under the assumption of Maxwellian electron energy distribution function (EEDF). n_i equals n_e in an electrically neutral plasma. The FHP method was first demonstrated in fusion plasma diagnostics[10-12] and has also been applied in low-temperature plasma diagnostics.[13] The feasibility of feedback control of plasma density based on continuous FHP measurement has been experimentally verified to achieve advanced plasma-process control.[14]

Since the FHP method can measure parameters even when there is a dielectric on the probe surface, it has attracted interest as a tool for parameter monitoring in reactive plasmas. To establish reactive plasma monitoring, FHP measurements with dielectric-coated probes were compared with the DC-based probe without the dielectric coating.[13,15] The FHP method was used to measure T_e and n_i during a process of deposition of a diamond-like carbon film.[16,17] Zanáška *et al.* investigated the influence of the dielectric-film thickness on the FHP measurement and recorded the temporal changes of T_e and n_i during iron-oxide film deposition.[18] In addition to the continuous deposition processes, Sato *et al.* monitored the temporal changes of T_e and n_i in a cyclic deposition process of silicon nitride films with a repeated pulsed discharge process.[19] These studies suggest that the FHP method is a suitable tool for monitoring and controlling advanced reactive-plasma processes.

Our study of the FHP method has two objectives. One is to quantitatively evaluate the stray impedances in the FHP system and their influence on the measurement. Current flowing to the ground through stray impedances is a common problem in AC-based electrical instruments. In previous studies, the probe-current amplitude measured without plasma generation was subtracted from the amplitude measured in plasma.[15,18] Choi *et al.* analyzed the influence of the stray capacitance by applying AC voltages with different frequencies to the probe.[20] By applying AC voltages with two frequencies and analyzing the current components at summation and differential frequencies the influence of stray capacitance was avoided.[21,22] In this study, we measured the stray impedances emanating from each component of the measurement system and additionally considered the capacitance formed by a plasma around the probe. Quantitative evaluation of the stray impedances improved the accuracy of the FHP measurements, especially under low-plasma-density conditions.

The main objective of this study was to perform FHP measurements without assuming a Maxwellian EEDF. This extends the applicable plasma sources and the range of discharge conditions of the FHP method. Previously, FHP methods modified with the theoretical background of an AC-superposition method in the LP measurement[3,23] has diagnosed effective electron temperatures T_{eff} in plasmas with non-Maxwellian EEDFs.[24,25] Our approach has been to establish an evaluation procedure for T_{eff} and n_{i} in non-Maxwellian-EEDF plasmas without the need for a small-amplitude approximation, required by the AC-superposition method. The lack of this approximation allows us to apply an AC voltage with a relatively large amplitude. This novel approach contributes to the accurate measurement of amplitudes of the harmonic currents. The applied voltage had a single frequency, and a lock-in amplifier was used to determine the amplitudes and phases of the probe current at the first, second, and third-harmonic frequencies. Using these three current amplitudes, we estimated the EEDF shape, T_{eff}, and n_i. Multi-harmonic analysis of the FHP data considering the stray impedances was performed in two low-temperature plasma sources: a surface-wave plasma (SWP) and an inductively coupled plasma (ICP) generated in a low-pressure argon (Ar) atmosphere.

2. Floating harmonic probe (FHP) method

2.1 Conventional analysis for Maxwellian-EEDF plasmas

Figure 1(a) shows the basic components of the FHP method. When an AC voltage is applied to a probe inserted in the plasma using an electric circuit with a blocking capacitor, the voltage at probe V_{pr} becomes

$$V_{\mathrm{pr}} = (V_{\mathrm{f}} + V_{\mathrm{dc}}) + V_0 \cos \omega t \qquad (1)$$

where V_f is the floating potential; V_{dc} is the DC self-bias voltage; V_0 and ω are the amplitude and angular frequency, respectively, of the applied AC voltage. The current flowing in the probe i_{pr} near V_f is composed of an ion saturation current i_{is} and an electron current i_e. The ion current was assumed to be constant at i_{is} in the range of the V_{pr}. i_e is determined by the electron saturation current i_{es}, the plasma potential V_{pl}, the V_{pr}, and the electron temperature T_e, when the EEDF in the tested plasma source is a Maxwellian distribution, as follows:

$$i_{\mathrm{pr}} = i_{\mathrm{is}} - i_{\mathrm{e}} = i_{\mathrm{is}} - i_{\mathrm{es}} \exp\left\{-\frac{V_{\mathrm{pl}} - V_{\mathrm{pr}}}{T_{\mathrm{e}}}\right\} \qquad (2)$$

T_e is assumed in units of eV in this and all following formulas. Due to the presence of a blocking capacitor, the DC component in i_{pr} is zero. i_{pr} can be expressed by the summation of the AC electron current components at harmonic frequencies of the **R-1** applied voltage $i_{e\_k\omega}$ as shown in Fig. 1(b). In the Maxwellian-EEDF case, the amplitude ratio of the electron current components of the first 1ω and second-harmonic 2ω frequencies, $i_{e\_1\omega}$ and $i_{e\_2\omega}$, is correlated with T_e as

$$\frac{|i_{e\_1\omega}|}{|i_{e\_2\omega}|} = \frac{I_1(V_0/T_e)}{I_2(V_0/T_e)} \qquad (3)$$

where $I_j(z)$ is the j^{th} modified Bessel function.[11)] The ion density n_i can be calculated using the following relationship:

$$n_i = \frac{|i_{e\_1\omega}|}{2(0.61 q_e u_B A)} \frac{I_0(V_0/T_e)}{I_1(V_0/T_e)} \qquad (4)$$

where, q_e is the elementary charge, u_B is the Bohm velocity, and A is the surface area of the probe tip.[13)] Using these relationships (Eq. (3) and (4)), the FHP method achieves a continuous output of the electron temperature T_e and the ion density n_i by monitoring $i_{e\_1\omega}$ and $i_{e\_2\omega}$. We refer to this conventional analysis method as “CA-FHP” in subsequent sections.

2.2 Multi-harmonic analysis for non-Maxwellian-EEDF plasmas

In the case of non-Maxwellian-EEDF plasma, we consider the following form of EEDF $g_e(\varepsilon)$ in this study.[26,27)]

$$g_e(\varepsilon) = g_X \frac{\sqrt{\varepsilon}}{(q_e T_{eff})^{3/2}} \exp\left\{-C_X \left(\frac{\varepsilon}{q_e T_{eff}}\right)^X\right\} \qquad (5)$$

where g_X and C_X are constants normalizing the EEDF, ε is the electron energy, and T_{eff} is the effective electron temperature. ε and T_{eff} are assumed in units of eV in this and all following formulas. **R-2** When X = 1 and X = 2, $g_e(\varepsilon)$ becomes the Maxwellian and Druyvesteyn distributions, respectively.

The electron current i_e as a function of voltage $V = V_\mathrm{pl} - V_\mathrm{pr}$ is expressed using $g_\mathrm{e}(\varepsilon)$ as follows:

$$i_\mathrm{e}(V) = \frac{q_\mathrm{e} n_\mathrm{e} A}{4} \int_{q_\mathrm{e}V}^{\infty} \left(1 - \frac{q_\mathrm{e}V}{\varepsilon}\right) \sqrt{\frac{2\varepsilon}{m_\mathrm{e}}}\, g_\mathrm{e}(\varepsilon) \mathrm{d}\varepsilon \qquad (6)$$

where m_e is the mass of the electron. When the AC voltage is applied, as shown in Fig. 1(b), the probe current i_pr becomes

$$i_\mathrm{pr} = i_\mathrm{is} - i_\mathrm{e}\Big(V_\mathrm{pl} - (V_\mathrm{f} + V_\mathrm{dc} + V_0 \cos \omega t)\Big) = i_\mathrm{is} - i_\mathrm{e}(t) \qquad (7)$$

The electron current i_e can be expanded in a Fourier series with harmonic amplitudes of

$$i_{\mathrm{e}\_k\omega} = \frac{\omega}{2\pi} \int_0^{\frac{2\pi}{\omega}} i_\mathrm{e}(t) \cos(k\omega t)\, \mathrm{d}t \qquad (8)$$ **R-3**

The ratio of the electron current amplitudes between the first and k^th harmonic frequencies at the probe voltage becomes:

$$\frac{\left|i_{\mathrm{e}\_k\omega}\right|}{\left|i_{\mathrm{e}\_1\omega}\right|} = \frac{\int_0^{2\pi/\omega} \left[\int_{q_\mathrm{e}V}^{\infty} (\varepsilon - q_\mathrm{e}V) \exp\left\{-C_X \left(\frac{\varepsilon}{q_\mathrm{e}T_\mathrm{eff}}\right)^X\right\} \mathrm{d}\varepsilon\right] \cos(k\omega t)\, \mathrm{d}t}{\int_0^{2\pi/\omega} \left[\int_{q_\mathrm{e}V}^{\infty} (\varepsilon - q_\mathrm{e}V) \exp\left\{-C_X \left(\frac{\varepsilon}{q_\mathrm{e}T_\mathrm{eff}}\right)^X\right\} \mathrm{d}\varepsilon\right] \cos(\omega t)\, \mathrm{d}t} \qquad (9)$$

This ratio includes three variable parameters: the DC component in V, i.e., $\langle V \rangle = \langle V_\mathrm{pl} - V_\mathrm{pr} \rangle = V_\mathrm{pl} - (V_\mathrm{f} + V_\mathrm{dc})$, X, and T_eff. **R-4** These can be determined using the numerical fitting of Eq. (9), with a set of harmonic currents from $|i_{\mathrm{e}\_1\omega}|$ to $|i_{\mathrm{e}\_4\omega}|$. In this study, since it was difficult to detect the $i_{\mathrm{e}\_4\omega}$ signal in our experimental system, we determined the voltage $V_\mathrm{FHP} = V_\mathrm{pl} - V_\mathrm{f}$ using the following equation,[2)]

$$V_\mathrm{FHP} = V_\mathrm{pl} - V_\mathrm{f} = \frac{T_\mathrm{e}}{2} + T_\mathrm{e} \ln\left(\sqrt{\frac{m_\mathrm{i}}{2\pi m_\mathrm{e}}}\right) \qquad (10)$$

where m_i is the ion mass. T_e in the calculation was derived using the CA-FHP method (Eq. (3)) from $|i_{\mathrm{e}\_1\omega}|$ and $|i_{\mathrm{e}\_2\omega}|$. Using the $V_\mathrm{FHP} + V_0 \cos\omega t$ as V in Eq. (9), and assuming **R-5** that V_{dc} is negligible, X and T_{eff} are determined from $|i_{e\_1\omega}|$, $|i_{e\_2\omega}|$, and $|i_{e\_3\omega}|$. We compared V_{FHP} with $V_{IV} = V_{pl} - (V_f + V_{dc})$ which results from by fitting the I–V characteristics for each measurement.

After determining X and T_{eff} using the V_{FHP} and Eq. (9), n_i can be calculated as follows:

$$n_i = \frac{|i_{e\_1\omega}|}{2(0.61 q_e u_B A)} \frac{|i_{e\_0\omega}|}{|i_{e\_1\omega}|} \qquad (11)$$ **R-6**

It should be noted that the above procedure for calculating V_{FHP} (Eq. (10)), and n_i (Eq. (11)) are based on the Maxwellian EEDF. The feasibility of the V_{FHP} and n_i calculation in the multi-harmonic analysis is discussed in Section 4.2 comparing with the parameters obtained from the I–V characteristics. Through the multi-harmonic analysis of the FHP data, called "MHA-FHP" in the following sections, we are able to investigate the parameters in non-Maxwellian-EEDF plasmas.

3. Experimental setup

3.1 Low-temperature plasma sources

Schematic representations of the SWP and ICP sources measured in this study are shown in Figs. 2(a) and 2(b), respectively. Two vacuum chambers with the same dimensions and materials were used for each plasma source. The SWP source (Fig. 2(a)) had a microwave antenna mounted on a quartz plate at the top of the chamber. The **R-7** microwave frequency was approximately 1 GHz. The discharge was performed 10-Pa Ar gas at a flow rate of 10 sccm. The ICP source (Fig. 2(b)) consisted of a 6-turn coil on a quartz plate connected to a matching box. The RF frequency was 13.56 MHz. The Ar **R-7** pressure and flow rate were 2.7 Pa and 10 sccm, respectively. The discharge gap between the quartz plate and the substrate stage, which was electrically floated in this study, was 130 mm.

As baseline data for the FHP measurements, we analyzed EEDF, V_{pl}, and V_f in the SWP and ICP sources using the *I*–*V* characteristics of a tungsten (W) probe obtained by the conventional LP method. The W probe tip had a cylindrical shape with a length of 1.0 mm and a diameter of 1.5 mm. The probe was placed on the central axis of the chamber, 10 mm above the stage. The distance between the quartz plate to the probe was long enough to measure the parameters without the influence of microwave and RF fields.[28,29] Figure 3 shows EEDFs measured in the SWP (Fig. 3(a)) and ICP (Fig. 3(b)), **R-12** which were calculated from the measured *I*–*V* characteristics using the Druyvesteyn method.[5,30] We analyzed the EEDF shape in a range over 10^{13} $eV^{-1}m^{-3}$ in this study. In general, under our discharge conditions, the SWP exhibited more Maxwellian-like EEDFs and lower average electron energy than ICP. The EEDFs measured with ICP showed Druyvesteyn-like shapes. The influence of the EEDF shape difference between SWP and ICP on the FHP measurement is discussed in the following sections. We also plotted V_{pl} and V_f of each plasma source in Figs. 4(a) and 4(b). In addition to the **R-9** voltages obtained from the *I*–*V* characteristics (V_{pl_IV} determined by a tangent method and V_{f_IV}), the voltage V_{pl_Druy} where the second derivative of the *I*–*V* curve becomes zero is also plotted as a plasma potential calculated without assuming Maxwellian EEDF.

3.2 FHP measurement

Figure 5 shows a diagram of the FHP measurement system used in this study. We applied an AC sinusoidal voltage $V_0\cos\omega t$ through a function generator. The amplitude (V_0 = 2.5 V) and frequency ($f = \omega/2\pi$ = 15.5 kHz) of the AC voltage are fixed. The current-sensing resistor R_s and the blocking capacitor C_b were R_s = 10 Ω and C_b = 10 μF, respectively. The lock-in amplifier measured the amplitudes (amp.) and phases (θ) of $i_{e\_k\omega}$ from the differential AC voltage between the two ends of R_s. A TTL signal from the function generator is also input to the lock-in amplifier as a frequency reference. The probe inserted into the chamber had a W tip with the same dimensions and positions as in the LP measurement. An Al_2O_3 tube with inner and outer diameters of 2.1 and 4.1 mm covered the W rod to control the length of the probe tip. In this study, a 49 mm long Al_2O_3 tube was exposed to plasma, and the rest of the probe in the chamber was covered with a grounded stainless-steel tube. From the V_0, V_f, and I–V characteristics, we calculated the DC self-bias voltages V_{dc_IV} under the AC-voltage applied to the probe. The $|V_{dc\_IV}|$ values for each discharge condition are plotted in Figs. 4(a) and 4(b).

To evaluate AC currents that do not flow through the ion sheath during the FHP measurement, we analyzed the stray impedances of each component at a frequency of 15.5 kHz. The impedances of each component, such as coaxial cable and connector, were measured using an LCR meter. The specification values of the input impedance of the lock-in amplifier were also considered. Following this procedure, we simulated amp. and θ at the lock-in amplifier at 15.5 kHz without plasma generation. The simulated values considering the measurement system circuit shown in Fig. 6 are amp. = 71.9 μA and θ = 89.8°. The experimentally measured output of the lock-in amplifier without plasma generation was amp. = 70.5 μA and θ = 89.1°, from which we conclude that the impedance rating was appropriate. The generation of additional impedance components must be considered in plasma diagnostics. These are the ion sheath, a parallel of C_{sh} and R_{sh}, and a capacitance between the W rod and the plasma separated by the Al_2O_3 tube, C_{st_pl}, as shown in Fig. 6. C_{sh} was negligible in our experimental setup, given the probe-tip area and the estimated sheath thickness. R_{sh} is a nonlinear resistance that was investigated in this study. We calculated the additional capacitance C_{st_pl} = 6.6 pF from the dimensions and relative permittivity of the Al_2O_3 material at ε_r = 9.[31] The calculated plasma parameters with and without considering the stray impedances were compared to investigate their influence on the FHP measurement in the following section.

4. Results and discussion

4.1 Surface-wave plasma (SWP) diagnostics

We diagnosed the SWP plasma in a range of microwave powers from 50 to 200 W using the FHP method. The measurement results of $i_{e\_k\omega}$ (k = 1, 2, 3) are summarised in Table I. For the first-harmonic frequency component (1ω) of the probe current, it must be taken into account that the current flowing to the stray impedances is included in the measured amplitude and phase ($i_{total\_1\omega}$ in Table I). Therefore, we subtracted the first-harmonic component measured without plasma generation and the estimated current flowing to C_{st_pl} from the $i_{total\_1\omega}$ measured at each microwave power to deduce the electron current flowing to the ion sheath ($i_{e\_1\omega}$).

Before calculating the electron energy, we estimated a DC component in the voltage **R-10**
V, i.e., $\langle V \rangle = \langle V_{pl} - V_{pr} \rangle = V_{pl} - (V_f + V_{dc})$, using the FHP method. The V_{FHP} values **R-11**

were calculated using Eq. (10) from $|i_{e\_2\omega}|/|i_{e\_1\omega}|$ (section 2.2). $V_{IV} = V_{pl\_IV} - (V_{f\_IV} + V_{dc\_IV})$ is derived from the data shown in Fig. 4(a). Figure 7 shows V_{FHP} and V_{IV} measured for each microwave power. It was confirmed that the V_{FHP} values similar to those of V_{IV}. This result indicates that when estimating the voltage V by the FHP method, assuming the Maxwellian EEDF and ignoring V_{dc} do not cause critical errors, at least when measuring the SWP.

Then, using the ratios $|i_{e\_2\omega}|/|i_{e\_1\omega}|$ and $|i_{e\_3\omega}|/|i_{e\_1\omega}|$ and the procedures explained in Eq. (9), we calculated X and T_{eff} for each microwave power using the V_{FHP}. The calculated X values, $X_{MHA\text{-}FHP}$, are shown in Fig. 8. The X values estimated from the EEDFs derived using the Druyvesteyn method X_{Druy} are also plotted. The details of the X_{Druy} estimation procedure can be found in the Appendix. The X values obtained by both methods were close to one. Therefore, the SWP measured in this study can be categorized as a Maxwellian-EEDF plasma, and the MHA-FHP method can adequately represent the Maxwellian property of the SWP.

The parameters T_{eff} and n_i determined by the MHA-FHP method ($T_{eff\_MHA\text{-}FHP}$ and $n_{i\_MHA\text{-}FHP}$) are shown in Figs. 9(a) and 9(b). For comparison, in Fig. 9(a) also shows T_e values calculated using the CA-FHP method (analysis in section 2.1) with ($T_{e\_CA\text{-}FHP}$) and without ($T_{e\_CA\text{-}FHP\_SI}$) consideration of the stray impedances. The influence of stray impedances on the measurement results increases lower microwave powers. This is because the ratio of $|i_{e\_1\omega}|/|i_{total\_1\omega}|$ decreases at low power due to the increase in the ion-sheath impedance. This suggests that the proper consideration of stray impedances extends the measurable lower limit of n_i in the FHP method. The $T_{eff\_MHA\text{-}FHP}$ and $T_{e\_CA\text{-}FHP,}$ which take the stray impedances into account, are consistent with the T_{e_IV} measured from 70 to 200 W using the conventional LP method. The deviation of

$T_{eff\_MHA\text{-}FHP}$ from $T_{e\_CA\text{-}FHP}$ and T_{e_IV} was observed for the 50-W data. This probably due to an error in the calculation caused by the low signal amplitude (low signal-to-noise ratio) at the third-harmonic frequency (3ω). In the n_i calculation results shown in Fig. 9(b), it can be observed that the CA-FHP method which ignores the stray impedances ($n_{i\_CA\text{-}FHP\_SI}$) significantly overestimates n_i since it is proportional to $|i_{e\_1\omega}|$ in the analysis of the FHP method based on Eq. (4).

4.2 Inductively coupled plasma (ICP) diagnostics

ICP generated with RF powers in the range of 50–200 W was diagnosed by the FHP method with procedures similar to those used for the diagnostics of SWP. The measurement results of $i_{total\_1\omega}$ and $i_{e\_k\omega}$ are summarized in Table II.

Figure 10 shows the DC component of the voltage V estimated based on the results of the FHP measurement V_{FHP} and the I–V characteristic V_{IV}. Although the ICP has a more Druyvesteyn-like EEDF compared to the SWP, as explained in Section 3.1, the V_{FHP} calculation assuming a Maxwellian EEDF shows good agreement with the V_{IV}. Therefore, we used the $V_{FHP,}$ calculated using the same procedure as the SWP, to further investigate the parameters of the ICP.

We have plotted the X values calculated from the ratios of $|i_{e\_2\omega}|/|i_{e\_1\omega}|$ and $|i_{e\_3\omega}|/|i_{e\_1\omega}|$ (Eq. (9)) and the V_{FHP} in Fig. 11. The values of $X_{MHA\text{-}FHP}$ are approximately two and agree with the X_{Druy} obtained from the I–V characteristics. This confirms that the assumption of a Maxwellian EEDF in the V_{FHP} calculation (Eq. (10)) does not significantly affect the EEDF-shape analysis and the subsequent calculation of the plasma parameters. The measured X values in the ICP were larger than those in the

SWP, i.e., more Druyvesteyn-like EEDFs, as indicated in Fig. 3. This result suggests that the MHA-FHP method can quantitatively distinguish the difference in plasma properties between SWP and ICP in terms of EEDF shape.

The T_{eff} values calculated by the MHA-FHP method using the V_{FHP} and $X_{MHA\text{-}FHP}$ for each RF power are shown in Fig. 12(a), along with the parameters calculated based on the CA-FHP, LP, and Druyvesteyn methods. The $T_{eff\_MHA\text{-}FHP}$ values were higher than $T_{e\_CA\text{-}FHP}$ values under each discharge condition. For the values calculated based on the I–V characteristics, T_{eff_Druy} was higher than T_{e_IV}. This suggests that the analyses assuming the Maxwellian EEDF underestimate the average electron energy in the plasmas that have a Druyvesteyn-like EEDF, as in our ICP case. The MHA-FHP method is necessary to obtain accurate information about the electron energy in such plasma sources. The n_i calculation results obtained with T_{eff} or T_e are shown in Fig. 12(b). All three analyses of n_i gave similar values for each RF power. This suggests that the n_i calculation based on Eq. (11) is suitable for diagnosing plasmas with a Druyvesteyn-like EEDF. The n_i values also suggested that the RF field does not have significant influence on the probe measurement. The longest skin depth in the discharge conditions calculated assuming $n_e = n_i$ was 37 mm, which was significantly shorter than the distance between the probe and the quartz plate (120 mm). **R-8**

From the experimental results, we conclude that the multi-harmonic analysis of FHP data (MHA-FHP method) has the potential to evaluate and monitor the EEDF shape and electron energy in low temperature plasmas. The monitoring of the EEDF shape is a feature of the MHA-FHP method that has potentials to contribute in further investigation of reactive plasmas with modulation of input power and/or gas-flow switching during the operation.

5. Conclusions

This paper presents our experimental studies on a method to accurately measure electron energy and ion density in low-temperature plasmas using a floating harmonic probe (FHP). An equivalent circuit analysis focusing on stray impedances in the FHP system has shown that data analyses without considering the stray impedances have overestimated the electron energy and ion density, especially under low-plasma-density conditions. We also discuss the influence of the electron energy distribution function (EEDF) on the FHP measurement when it deviates from the Maxwellian shape. For parameter estimation in plasmas that have not only Maxwellian but also Druyvesteyn-like EEDFs, we have proposed a new approach to multi-harmonic analysis that uses the first, second, and third harmonic components in the measured probe current, an MHA-FHP method. The MHA-FHP method provides the shape of the EEDF, effective electron temperature, and ion density. The EEDF shapes and effective electron temperatures obtained from the MHA-FHP measurement showed good agreement with parameters obtained from EEDFs derived by the Druyvesteyn method, in both surface-wave plasma (SWP, Maxwellian-like EEDFs) and inductively coupled plasma (ICP, Druyvesteyn-like EEDFs) diagnostics. This is a clear advantage of the MHA-FHP method compared to the conventional FHP and Langmuir probe methods, which require Maxwellian EEDF. From these experimental results and discussion, we conclude that the MHA-FHP method has the potential to be an important method for monitoring fundamental plasma parameters in various reactive plasma processes.

Acknowledgments

This work was supported financially in part by a Grant-in-Aid for Research Activity Start-up (18H05849) and Grant-in-Aid for Scientific Research (B) (19H01886) from the Japan Society for the Promotion of Science.

Appendix

Analysis of EEDF obtained by a Druyvesteyn method

In the following, we explain the procedure for estimating the coefficient X in the electron energy distribution function (EEDF), written in Eq. (5), and the effective electron temperature T_{eff} from the EEDF based on the Druyvesteyn method. First, we calculated an EEDF from the I–V characteristic of the probe, using the conventional Druyvesteyn method.[5,30] The calculated EEDFs for the SWP and ICP (both at 150 W) are shown as circles in Figs. A1(a) and A1(b). The calculated EEDFs are also plotted in Fig. 3. Here, we analyzed T_{eff} from the EEDFs considering the range of probe voltage at the FHP measurement for data comparison with the FHP. The ranges of the probe voltage in the FHP measurement, determined by V_f, V_{dc}, and V_0 (see section 2.1), are indicated as energy ranges where the data points are yellow in the figures. X and T_{eff} for the EEDFs were estimated by fitting the yellow-coloured data points using Eq. (5). The fitting results are indicated by red lines in Figs. A1(a) and A1(b), which represent the general characteristics of the EEDFs in each plasma source. The X and T_{eff} values derived from the data analysis are shown in Figs. 8 and 11 as X_{Druy} and Fig. 12(a) as T_{eff_Druy}, respectively. For the references, we also show lines of data fitting with Maxwellian (X = 1, blue dashed lines) and Druyvesteynian (X = 2, purple dashed-dotted lines) EEDFs for each data point.

References

1) I. H. Hutchinson, *Principles of Plasma Diagnostics* (Cambridge University Press, Cambridge, 2002) 2nd ed., p. 55.

2) M. A. Lieberman and A. J. Lightenberg, *Principles of Plasma Discharges and Materials Processing* (Wiley, New Jersey, 2005) 2nd ed., p. 185.

3) S. Teii, Purazuma Kiso Kougaku (Fundamental of Plasma Engineering) (Uchida Rokakuho, Tokyo, 1997) 2nd ed., p.212 [in Japanese].

4) H. Amemiya, M. Wada, H. Toyoda, K. Nakamura, A. Ando, K. Uehara, K. Oyama, O. Sakai, and K. Tachibana, J. Plasma Fusion Res. **81**, 482 (2005) [in Japanese].

5) V. A. Godyak, R. B. Piejak, and B. M. Alexandrovich, Plasma Sources Sci. Technol. **1**, 36 (1992).

6) H. Singh and D. B. Graves, J. Appl. Phys. **87**, 4098 (2000).

7) H. Kokura, K. Nakamura, I. P. Ghanashev, and H. Sugai, Jpn. J. Appl. Phys. **38**, 5262 (1999).

8) H. Sugai, J. Plasma Fusion Res. **78**, 998 (2002) [in Japanese].

9) K. Nakamura, M. Ohata, and H. Sugai, J. Vac. Sci. Technol. A **21**, 325 (2003).

10) G. Proudfoot and P. J. Harbour, J. Nucl. Mater. **93/94**, 413 (1980).

11) R. Van Nieuwenhove and G. Van Oost, Rev. Sci. Instrum. **59**, 1053 (1988).

12) J. A. Boedo, D. Gray, R. W. Conn, P. Luong, M. Schaffer, R. S. Ivanov, A. V. Chernilevsky, G. Van Oost, and The TEXTOR Team, Rev. Sci. Instrum. **70**, 2997 (1999).

13) M.-H. Lee, S.-H. Jang, and C.-W. Chung, J. Appl. Phys. **101**, 033305 (2007).

14) S.-H. Jang, S.-J. Oh, Y.-K. Lee, and C.-W. Chung, Curr. Appl. Phys. **13**, 76 (2013).

15) J.-Y. Bang, K. Yoo, D.-H. Kim, and C.-W. Chung, Plasma Sources Sci. Technol. **20**, 065005 (2011).

16) J. Pang, W. Lu, Y. Xin, H. Wang, J. He, and J. Xu, Plasma Sci. Technol. **14**, 172 (2012).

17) Y. Bai, J. Li, J. Xu, W. Lu, Y. Wang, and W. Ding, Plasma Sci. Technol. **18**, 58 (2016).

18) M. Zanáška, Z. Hubička, M. Čada, P. Kudrna, and M. Tichý, J. Phys. D: Appl. Phys. **51**, 025205 (2018).

19) M. Sato, T. Ikeda, and N. Yamamoto, Proc. 26th Workshop; IEEJ Yamanashi and East-Shizuoka Branches, YS.26-03 (2019) [In Japanese].

20) M.-S. Choi, S.-H. Lee, and G.-H. Kim, J. Korean Phys. Soc. **55**, 1841 (2009).

21) S.-H. Jang, G.-H. Kim, and C.-W. Chung, Thin Solid Films **519**, 7042 (2011).

22) D.-H. Kim, H.-C. Lee, Y.-S. Kim, and C.-W. Chung, Appl. Phys. Lett. **103**, 084103 (2013).

23) R. H. Sloane and E. I. R. MacGregor, Phil. Mag. **18**, 193 (1934).

24) J. Y. Bang, A. Kim, and C. W. Chung, J. Appl. Phys. **107**, 103312 (2010).

25) S.-R. Huh, N.-K. Kim, H.-J. Roh, M.-S. Choi, S.-H. Lee, and G.-H. Kim, J. Phys. D: Appl. Phys. **48**, 022001 (2015).

26) H. Amemiya, J. Phys. Soc. Jpn. **66**, 1335 (1997).

27) J. T. Gudmundsson, Plasma Sources Sci. Technol. **10**, 76 (2001).

28) J. Hopwood, C. R. Guarnieri, S. J. Whitehair, and J. J. Cuomo, J. Vac. Sci. Technol. A **11**, 147 (1993).

29) M. Nagatsu, G. Xu, I. Ghanashev, M. Kanoh, and H. Sugai, Plasma Sources Sci. Technol. **6**, 427 (1997).

30) V. A. Godyak and V. I. Demidov, J. Phys. D: Appl. Phys. **44**, 233001 (2011).

31) ed. National Astronomical Observatory of Japan, *Rika Nenpyo* (Chronological Scientific Tables) (Maruzen Publishing, Tokyo, 2015) p. 425 [in Japanese].

Figure Captions

Figure 1: Schematic representations of (a) the basic components and their arrangement for the FHP method and (b) the relationships between an applied AC voltage, a current-voltage (*I*–*V*) characteristic of the ion sheath, and a measured probe current used in the FHP measurement.

Figure 2 (Color online): Schematic representations of (a) surface-wave plasma (SWP) and (b) inductively coupled plasma (ICP) sources diagnosed in this study.

Figure 3: Electron energy distribution functions (EEDFs) of (a) the SWP and (b) the ICP calculated from the *I*–*V* characteristics using a Druyvesteyn method. The EEDFs measured with microwave and RF power at 150 W are plotted in Figs. A1(a) and A1(b). **R-12**

Figure 4: Plasma potentials V_{pl} and floating potentials V_f for (a) the SWP and (b) the ICP measured at different discharge powers. The DC self-bias voltages V_{dc} were calculated from the *I*–*V* characteristics considering the V_f and the amplitude of the applied AC voltage (V_0 = 2.5 V).

Figure 5: Schematic diagram of the FHP measurement system used in this study. A DC component in the probe current was blocked by a blocking capacitor C_b. The current components at fundamental and harmonic frequencies were measured using a lock-in amplifier operated in a differential mode.

Figure 6: Electrical circuit of the FHP measurement system. The components considered in the analysis were stray capacitances of cables/connectors (C_{st_1}, C_{st_2}, and C_{st_3}), a sensing resistor (R_s), a blocking capacitor (C_b), and an impedance of the lock-in amplifier's input. When we generate a plasma, we need to consider the impedance of the ion sheath (a parallel of C_{sh} and R_{sh}) and the capacitance between the W rod and the plasma separated by a Al_2O_3 tube (C_{st_pl}) .

Figure 7: DC component in the voltage V (= V_{pl} − V_{pr}) derived from the FHP method with an assumption of Maxwellian EEDF V_{FHP} and from the I–V characteristic V_{IV} measured in the SWP operated with microwave powers from 50 to 200 W.

Figure 8: Coefficient X values indicating the EEDF shape in Eq. (5) calculated by the multi-harmonic analysis of the FHP data $X_{MHA\text{-}FHP}$ and by fitting the EEDF derived by the Druyvesteyn method X_{Druy}, measured in the SWP operated with the microwave powers from 50 to 200 W.

Figure 9: (a) Electron energies (T_{eff}, T_e) and (b) ion densities (n_i) measured in the SWP, operated with the microwave powers from 50 to 200 W, with the FHP method using the multi-harmonic analysis ($T_{eff\_MHA\text{-}FHP}$ and $n_{i\_MHA\text{-}FHP}$) and conventional analyses with ($T_{e\_CA\text{-}FHP}$ and $n_{i\_CA\text{-}FHP}$) and without ($T_{e\_CA\text{-}FHP\_SI}$ and $n_{i\_CA\text{-}FHP\_SI}$) consideration of the stray impedances. The T_e and n_i derived from the I–V characteristics using the conventional LP method (T_{e_IV} and n_{i_IV}) are also plotted.

Figure 10: DC component in the voltage V (= V_{pl} − V_{pr}) derived from the FHP method with an assumption of Maxwellian EEDF V_{FHP} and from the I–V characteristic V_{IV} measured in the ICP operated with the RF powers from 50 to 200 W.

Figure 11: Coefficient X values indicating the EEDF shape in Eq. (5) calculated by the multi-harmonic analysis of the FHP data $X_{MHA\text{-}FHP}$ and by fitting of the EEDF derived by the Druyvesteyn method X_{Druy}, measured in the ICP operated at the RF powers from 50 to 200 W.

Figure 12: (a) Electron energies (T_{eff}, T_e) and (b) ion densities (n_i) measured in the ICP, operated with the RF powers from 50 to 200 W, with the FHP method using the multi-harmonic analysis ($T_{eff\_MHA\text{-}FHP}$ and $n_{i\_MHA\text{-}FHP}$) and conventional analyses considering the stray impedances ($T_{e\_CA\text{-}FHP}$ and $n_{i\_CA\text{-}FHP}$). The T_e and n_i derived by the LP method (T_{e_IV} and n_{i_IV}) and the T_{eff} derived from the EEDF as explained in the Appendix (T_{eff_Druy}) are also plotted.

Figure A1 (Color online): Electron energy distribution functions (EEDFs) of (a) the SWP and (b) the ICP calculated from the I–V characteristics by the Druyvesteyn method. The microwave and RF powers for both data were 150 W. Data points in a range of probe voltage in the FHP method (yellow-coloured circles) were used for the fitting with Eq. (5). The fitting results with Maxwellian (X = 1) and Druyvesteynian (X = 2) EEDFs are also shown for reference.

Table I: Measured data of the harmonic components in the probe (electron) current $i_{\mathrm{e}\_k\omega}$ used in the FHP method. The data were obtained in the SWP generated with the microwave powers listed on the left. $i_{\mathrm{e}\_1\omega}$ is an electron current component flowing to the ion sheath derived by subtracting the component measured without the plasma generation and the estimated current flowing to the $C_{\mathrm{st\_pl}}$ (amp. = 70.5 μA and θ = 89.1° in total) from the components measured in each microwave power ($i_{\mathrm{total}\_1\omega}$).

Microwave power (W)	$i_{\mathrm{total}\_1\omega}$		$i_{\mathrm{e}\_1\omega}$		$i_{\mathrm{e}\_2\omega}$		$i_{\mathrm{e}\_3\omega}$	
	amp. (μA)	θ (deg.)	amp. (μA)	θ (deg.)	amp. (μA)	θ (deg.)	amp. (μA)	θ (deg.)
50	86.9	55.0	48.7	0.9	21.8	359.3	7.3	358.9
70	95.7	48.2	62.7	0.8	28.8	359.3	9.6	358.9
100	109.7	40.6	82.3	0.6	38.4	359.3	12.5	359.1
150	133.7	32.1	112.2	0.3	52.7	359.3	17.1	359.0
200	160.6	26.2	143.1	0.2	66.9	359.2	21.8	358.8

Table II: Measured data of $i_{\mathrm{e}\_k\omega}$ obtained in the ICP with the RF powers listed on the left. The $i_{\mathrm{e}\_1\omega}$ is calculated in the same manner as the SWP case in Table I. A summation of the first-harmonic component measured without the plasma generation and the estimated current flowing to the $C_{\mathrm{st\_pl}}$ was amp. = 70.3 μA and θ = 88.8°.

RF power (W)	$i_{\mathrm{total}\_1\omega}$		$i_{\mathrm{e}\_1\omega}$		$i_{\mathrm{e}\_2\omega}$		$i_{\mathrm{e}\_3\omega}$	
	amp. (μA)	θ (deg.)	amp. (μA)	θ (deg.)	amp. (μA)	θ (deg.)	amp. (μA)	θ (deg.)
50	84.7	57.2	44.5	1.3	12.0	359.1	1.9	357.7
70	101.5	44.2	71.3	0.5	20.0	359.0	3.5	357.2
100	117.6	37.0	92.5	0.3	28.8	258.9	5.4	357.9
150	161.4	25.8	143.9	0.0	41.2	358.8	7.2	358.2
200	186.6	22.2	171.2	0.0	47.1	359.0	8.0	358.6

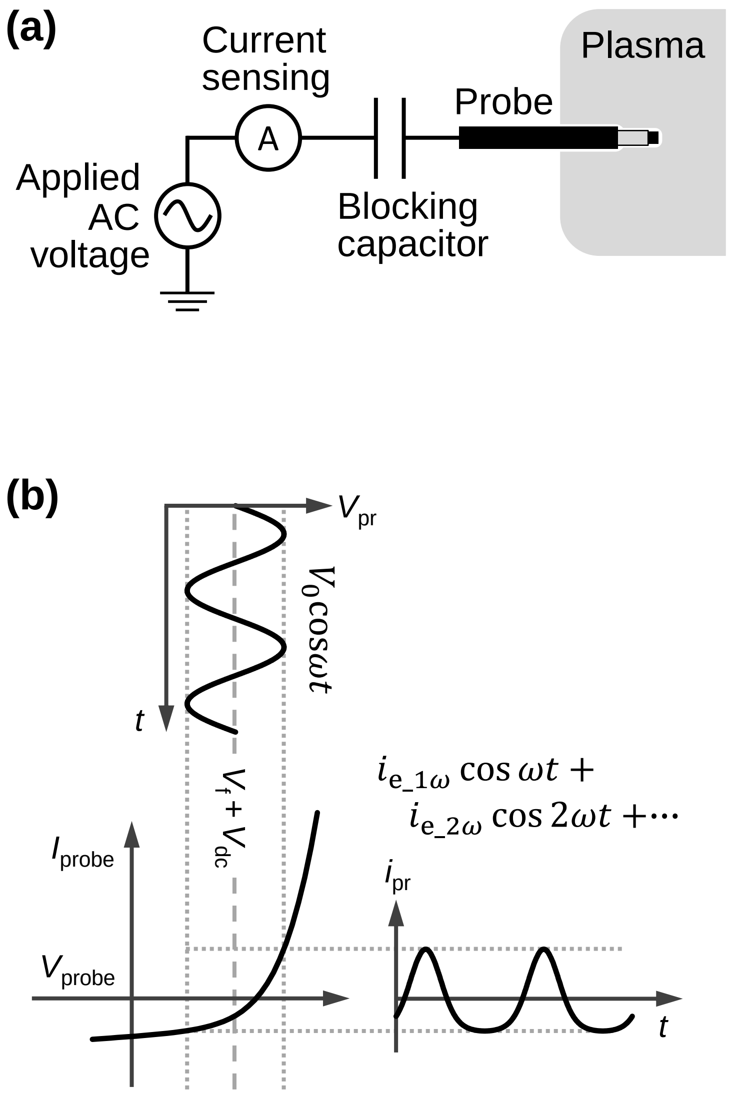
(a)
Current sensing
Plasma
Probe
A
Applied AC voltage
Blocking capacitor
(b)
V_{pr}
$V_0 \cos\omega t$
t
$V_f + V_{dc}$
$i_{e\_1\omega} \cos \omega t +$
$i_{e\_2\omega} \cos 2\omega t + \cdots$
I_{probe}
i_{pr}
V_{probe}
t

Figure 1

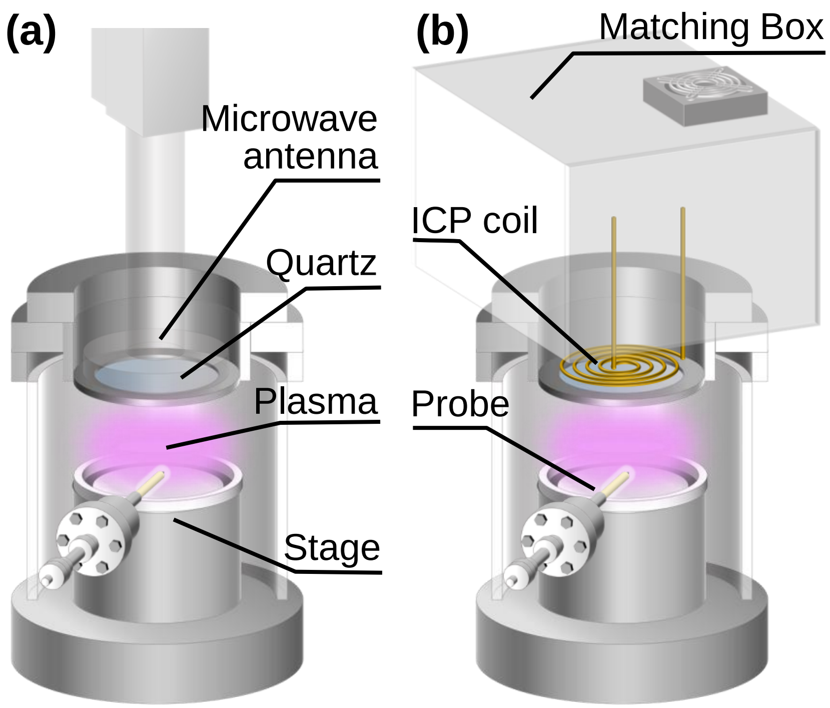

Figure 2 (Color online)

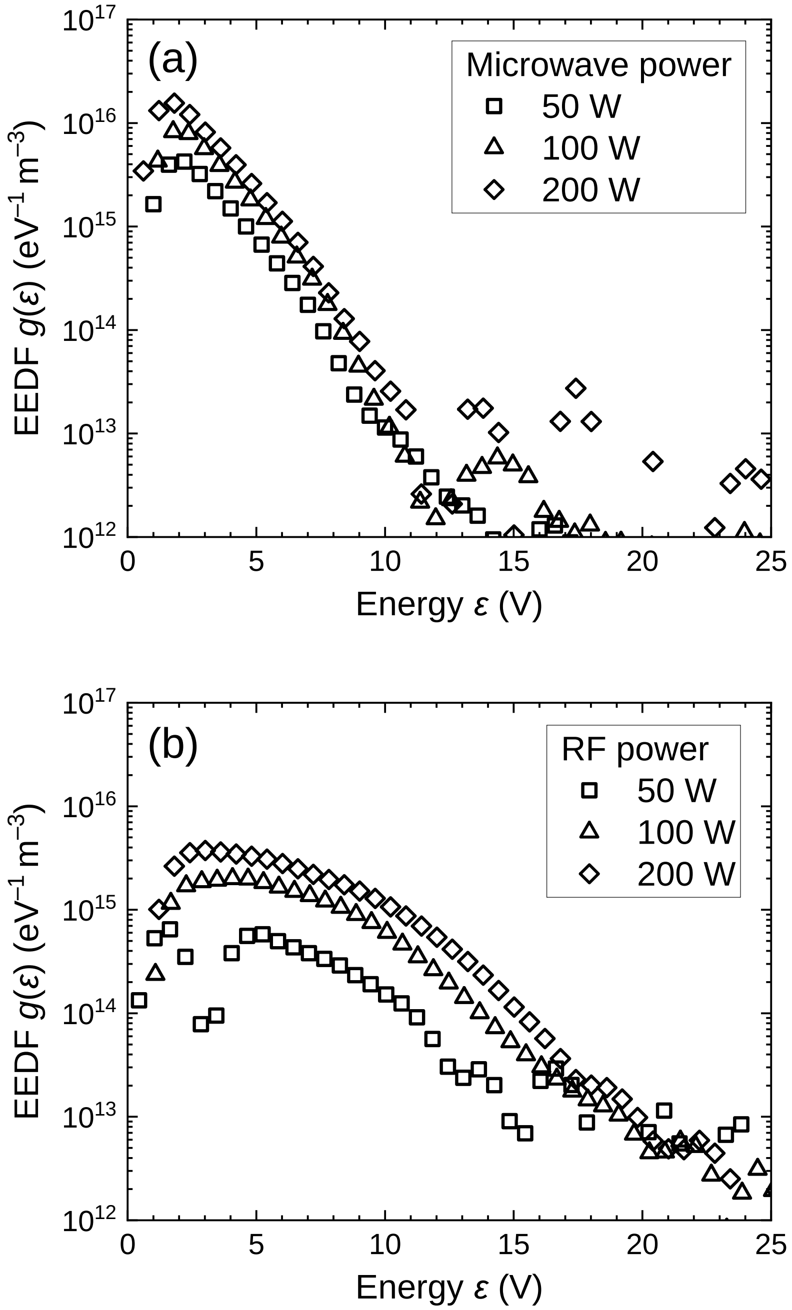
(a)
Microwave power
50 W
100 W
200 W
EEDF g(ε) (eV⁻¹ m⁻³)
Energy ε (V)
(b)
RF power
50 W
100 W
200 W
EEDF g(ε) (eV⁻¹ m⁻³)
Energy ε (V)

R-12

Figure 3

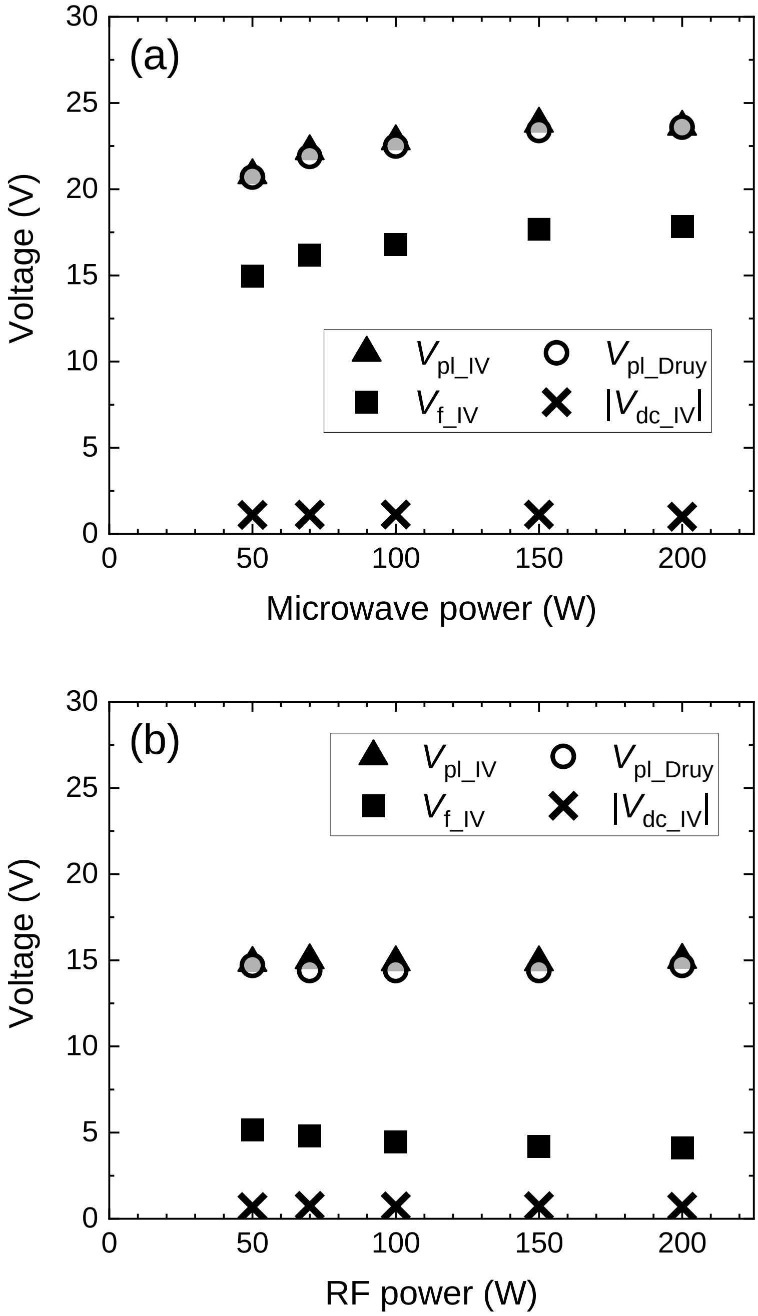
(a)
Voltage (V)
30
25
20
15
10
5
0
0
50
100
150
200
Microwave power (W)
V_{pl_IV}
V_{pl_Druy}
V_{f_IV}
$|V_{dc\_IV}|$
(b)
Voltage (V)
30
25
20
15
10
5
0
0
50
100
150
200
RF power (W)
V_{pl_IV}
V_{pl_Druy}
V_{f_IV}
$|V_{dc\_IV}|$

Figure 4

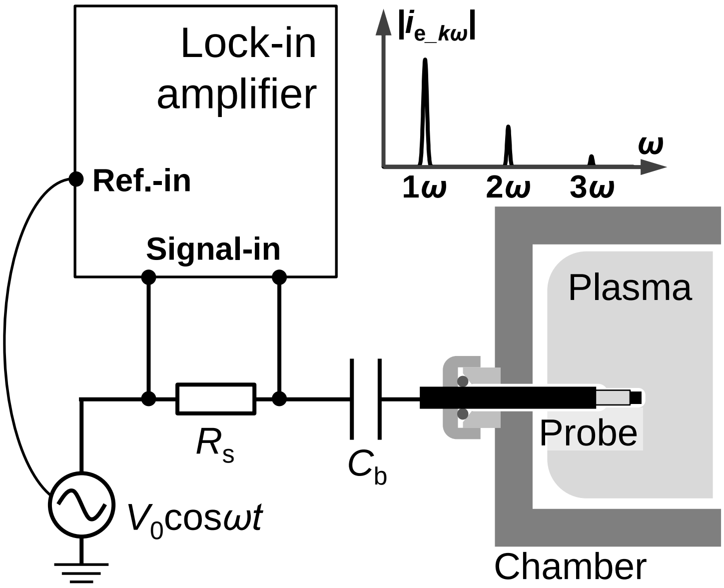

Lock-in amplifier
Ref.-in
Signal-in
|i_e_kω|
ω
1ω
2ω
3ω
Plasma
Probe
Chamber
Rs
Cb
V0cosωt

Figure 5

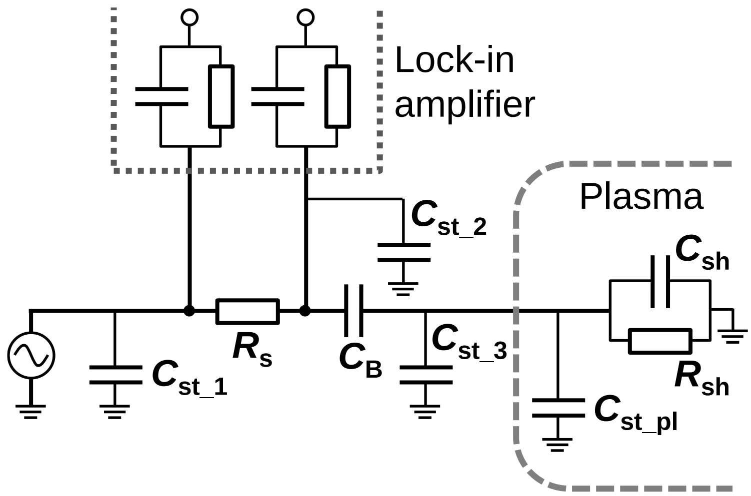

Figure 6

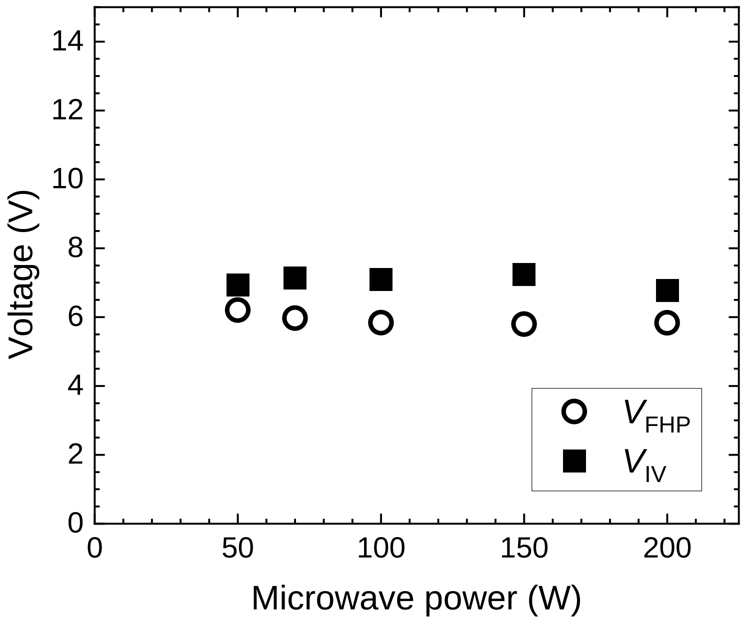

Voltage (V)
Microwave power (W)
V_{FHP}
V_{IV}
0
2
4
6
8
10
12
14
0
50
100
150
200

Figure 7

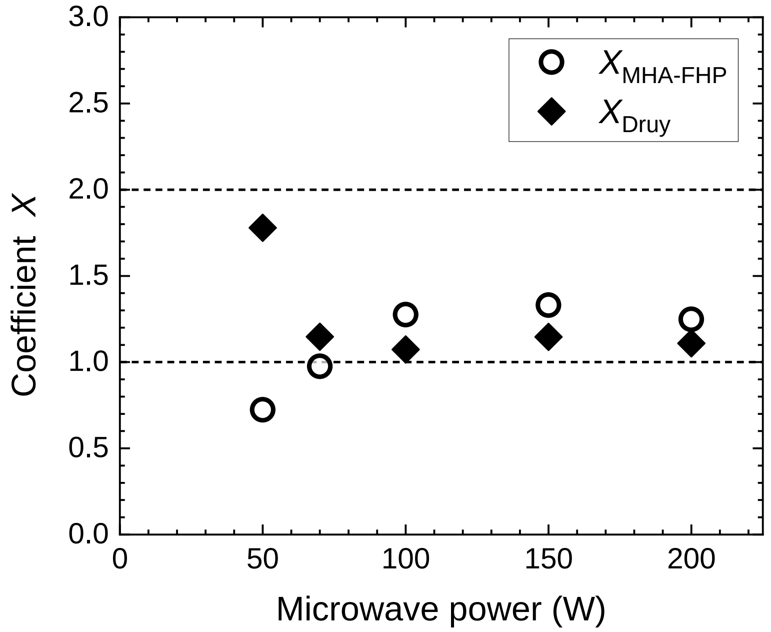
3.0
2.5
2.0
1.5
1.0
0.5
0.0
Coefficient X
0
50
100
150
200
Microwave power (W)
$X_{MHA-FHP}$
X_{Druy}

Figure 8

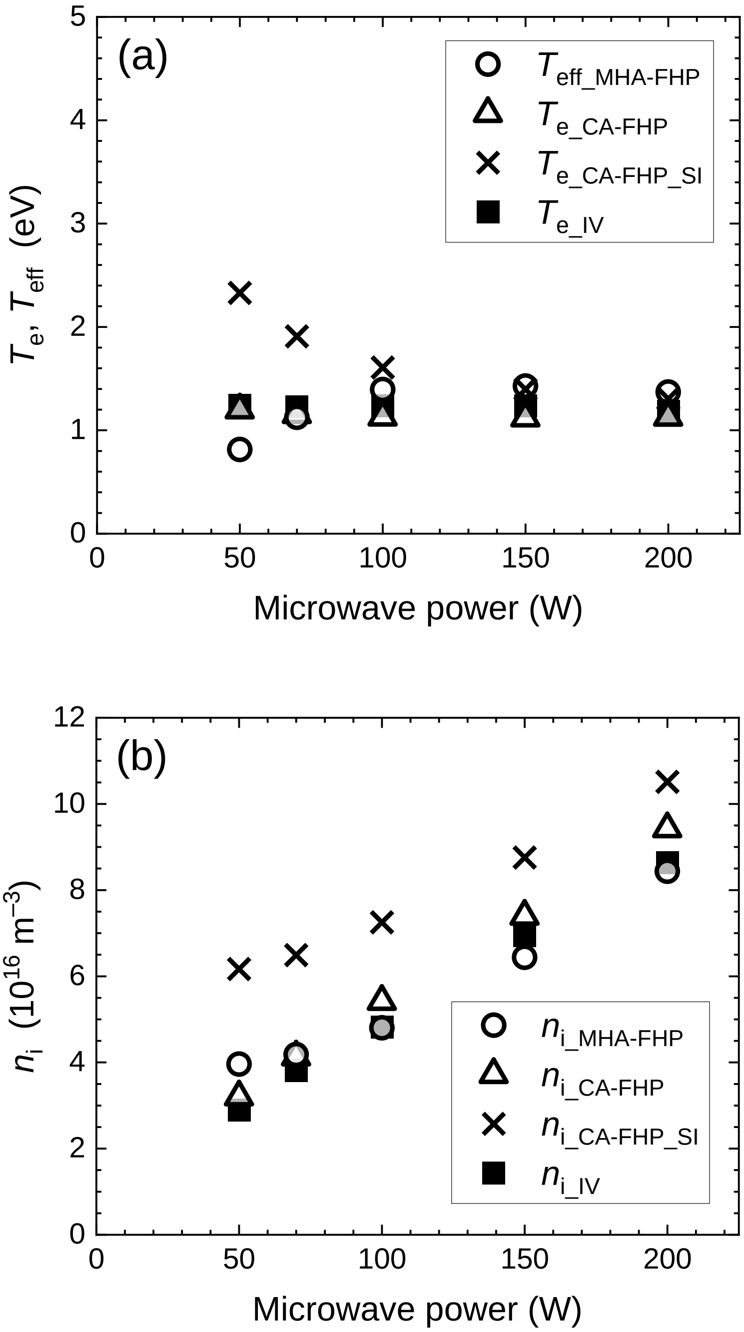
(a)
$T_{eff\_MHA\text{-}FHP}$
$T_{e\_CA\text{-}FHP}$
$T_{e\_CA\text{-}FHP\_SI}$
T_{e_IV}
T_e, T_{eff} (eV)
Microwave power (W)
(b)
$n_{i\_MHA\text{-}FHP}$
$n_{i\_CA\text{-}FHP}$
$n_{i\_CA\text{-}FHP\_SI}$
n_{i_IV}
n_i (10^{16} m^{-3})
Microwave power (W)

Figure 9

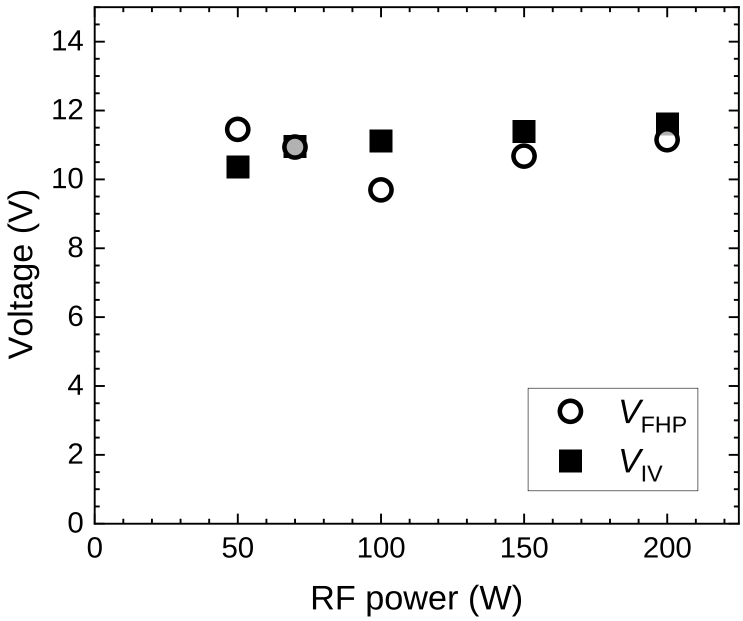

Figure 10

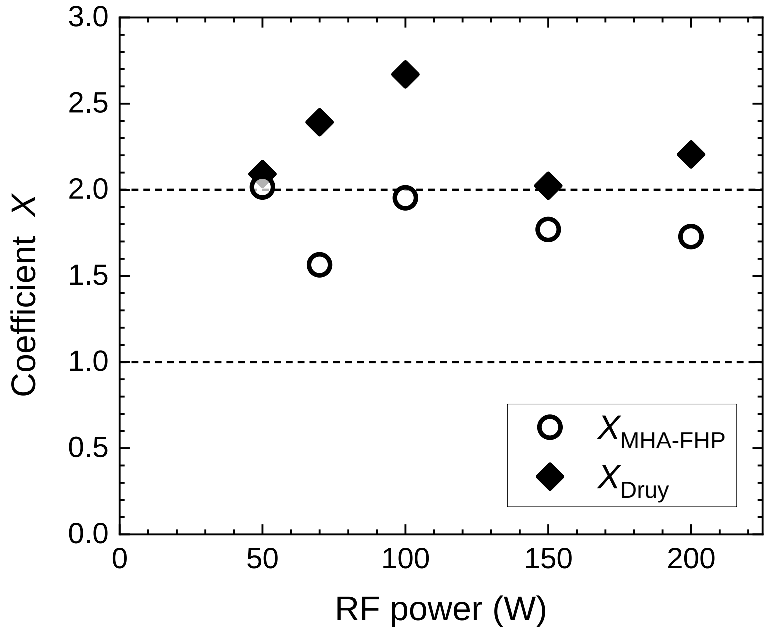
3.0
2.5
2.0
1.5
1.0
0.5
0.0
Coefficient X
0
50
100
150
200
RF power (W)
$X_{MHA-FHP}$
X_{Druy}

Figure 11

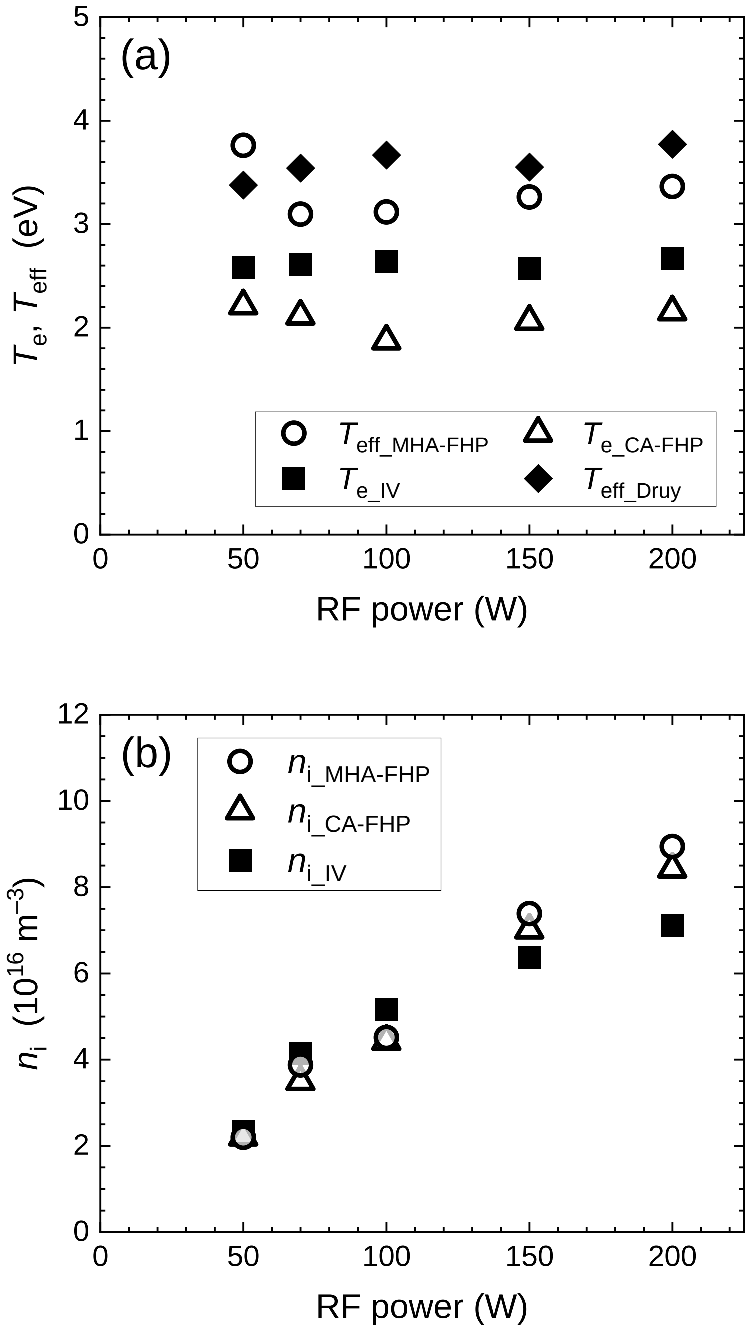
(a)
Te, Teff (eV)
RF power (W)
Teff_MHA-FHP
Te_CA-FHP
Te_IV
Teff_Druy
(b)
ni (10^16 m^-3)
RF power (W)
ni_MHA-FHP
ni_CA-FHP
ni_IV

Figure 12

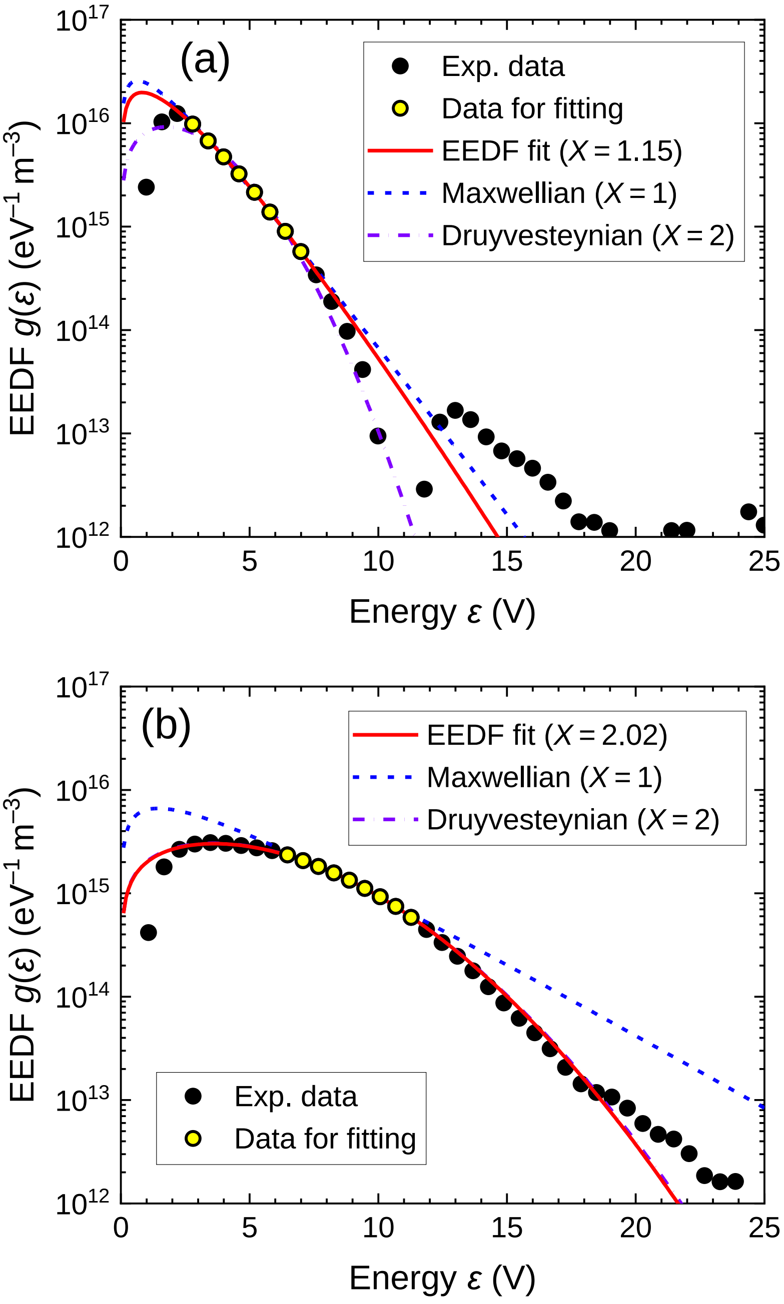

Figure A1 (Color online)